IOP PUBLISHING JOURNAL OF PHYSICS D: APPLIED PHYSICS

J. Phys. D: Appl. Phys. **41** (2008) 025103 (6pp) doi:10.1088/0022-3727/41/2/025103

Microstructure and electrical properties of p-type phosphorus-doped ZnO films

A Allenic[1], W Guo[1], Y B Chen[1], Y Che[2], Z D Hu[2], B Liu[2] and X Q Pan[1,3]

1 Department of Materials Science and Engineering, The University of Michigan, Ann Arbor, MI 48109, USA
[2] IMRA America, Inc., Ann Arbor, MI 48105, USA

E-mail: panx@umich.edu

Received 31 October 2007, in final form 1 November 2007
Published 21 December 2007
Online at stacks.iop.org/JPhysD/41/025103

Abstract
The microscopic defects and their effects on the electrical properties of phosphorus-doped ZnO films epitaxially grown on (0 0 0 1) sapphire and ZnO substrates by pulsed laser deposition are studied. While threading dislocations were observed only in heteroepitaxial films, a high density of partial dislocations associated with interstitial dislocation loops was observed in films grown on both substrates. These dislocations provide sinks to quench native donors and favour the injection of zinc vacancies to form acceptor-complex defects, thus leading to p-type conductivity.

1. Introduction

The breakthroughs in the growth and defect control of III–V semiconductor films have made possible the fabrication of high-brightness light-emitting heterostructures based on GaN and related alloys [1]. As a II–VI wide band gap semiconductor, ZnO is also a material of choice for short-wavelength optoelectronics [2]. The band gap of ZnO can be engineered via dilute alloying with CdO [3], MgO [4] and BeO [5]. The more tightly bound exciton in ZnO (59 meV) compared with other compound semiconductors (30 meV for GaN) opens the possibility for ZnO-based optical devices to operate well above 300 K (26 meV). Yet, the major bottleneck to the success of ZnO for optical device applications continues to be the lack of stable p-type material.

The greatest challenge towards p-type conductivity in ZnO lies in the understanding of its intrinsic and doping-induced defects. For example, the pinning effect of the dopant on the dislocation slip or the electrical passivation of the dopant by gettering can strongly affect the conductivity type of ZnO films [6, 7].

According to first principles calculations, doping ZnO with P_2O_5 under oxygen-rich conditions induces two acceptors, the zinc vacancy (V_{Zn}) and the P_{Zn}–$2V_{Zn}$ complex [8, 9]. The calculations predict that the formation and ionization energies of these two acceptors depend on the chemical potential of oxygen during growth. In a previous work, we tested these predictions for heteroepitaxial phosphorus-doped ZnO films grown on (0 0 0 1) sapphire and discussed how phosphorus and dislocations interact to create the P_{Zn}–$2V_{Zn}$ complexes responsible for p-type conductivity [10]. We observed a high density of threading dislocations induced by the large lattice mismatch between ZnO and sapphire, and by the small diffusivity of phosphorus atoms during growth. We also observed 10^{11}–10^{12} cm^{-2} Frank–Shockley partial dislocations associated with type-I interstitial stacking faults in films doped with 3.5×10^{20} P cm^{-3}. While the existence of a high density of threading dislocations enhanced the solubility of phosphorus in ZnO, both threading dislocations and stacking faults associated with interstitial dislocation loops facilitated the formation of zinc vacancies. The zinc vacancies were therefore the key defects responsible for the formation of P_{Zn}–$2V_{Zn}$ complexes and for the onset of p-type conductivity in PZO films following post-growth annealing.

Homoepitaxy has the advantage of reducing the density of crystal defects, offering potentially higher quantum efficiencies in multilayered ZnO optical devices. Thus, there is a strong motivation to study and understand the role of crystal defects on the conductivity type of homoepitaxial ZnO layers doped with phosphorus, and generalize the model discussed in [10].

[3] Author to whom any correspondence should be addressed.

 © 2008 IOP Publishing Ltd Printed in the UK

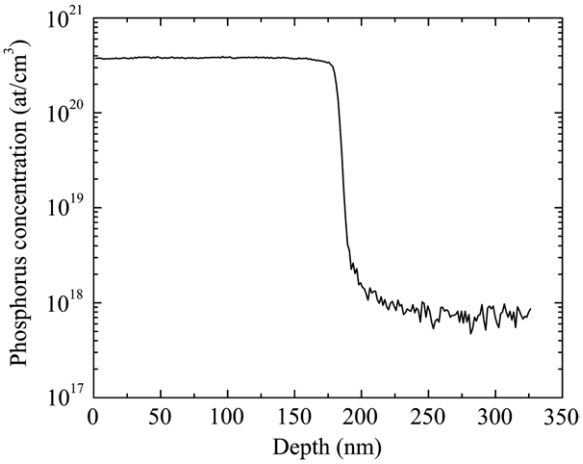

Figure 1. Secondary-ion mass spectroscopy of phosphorus in p-type homoepitaxial PZO.

2. Experimental

PZO films with thicknesses between 200 and 500 nm were deposited at 600 °C in 20 mTorr O_2 on both (0 0 0 1) sapphire and (0 0 0 1) Zn-polar ZnO substrates by pulsed laser ablation of a ZnO target doped with 1 wt.% P_2O_5. The growth rate was 1 Å s^{-1}. The microstructures and interfacial atomic structures of the PZO films were characterized by triple-axis x-ray diffraction (XRD) and transmission electron microscopy (TEM). The epilayer tilt angle (angle of rotation perpendicular to the growth plane) was determined by a Hall–Williamson analysis [11]; the epilayer twist angle (angle of rotation within the growth plane) was determined by rocking curve measurements of off-axis reflections in the skew symmetric diffraction geometry. The densities of dislocations with a screw- and with an edge-component were calculated from the mosaic angles using the formulas derived by Dunn and Koch [12]. Ti/Au and Ni/Au bilayers were used as the ohmic contacts to the n-type and p-type films. Low-temperature Hall-effect and photoluminescence measurements were conducted in a closed-cycle helium cryostat. The magnetic field was 0.23 T. The photoluminescence was excited with the 325 nm radiation of a 100 mW He–Cd laser, dispersed by a 1 m Jobin-Yvon spectrometer and detected by a photomultiplier tube operating in photon counting mode. The excitation intensity was set to 5×10^{-2} W cm^{-2}. The films grown on the (0 0 0 1) sapphire and the (0 0 0 1) ZnO substrates are referred to as heteroepitaxial and homoepitaxial films, respectively.

3. Results and discussion

3.1. Doping effect on the microstructure

Figure 1 shows the phosphorus depth profile measured by secondary-ion mass spectroscopy of a 185 nm thick homoepitaxial PZO film. A phosphorus-implanted sample was used as reference to convert the signal intensity into phosphorus concentration. It can be seen that phosphorus distributes uniformly with a concentration of 3.8×10^{20} cm^{-3} throughout the whole film. A similar result (3.5×10^{20} cm^{-3}) was obtained for the heteroepitaxial PZO films deposited under the same conditions [10].

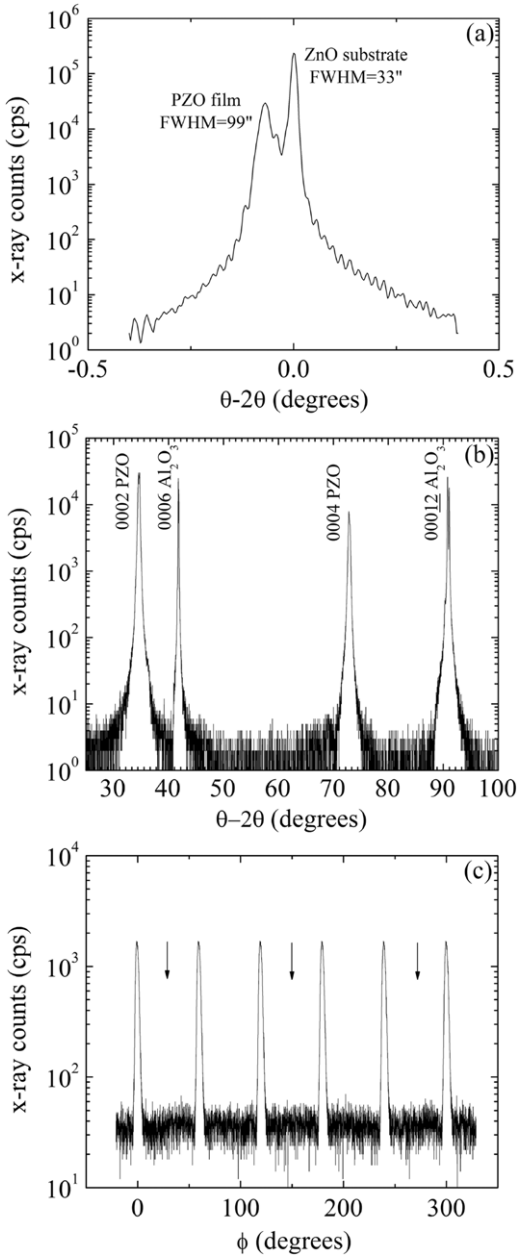

Figure 2. 0 0 0 2 θ–2θ XRD pattern of (*a*) p-type homoepitaxial PZO (FWHMs measured in arcsec) and (*b*) p-type heteroepitaxial PZO. (*c*) 1 1 $\bar{2}$ 4 ZnO ϕ-scan of p-type heteroepitaxial PZO. The arrows correspond to the substrate reflections.

The crystallinity of the PZO films grown on both the ZnO and the sapphire substrates was studied by XRD. Figure 2(*a*) shows a 0 0 0 2 θ–2θ XRD pattern of a homoepitaxial p-type PZO film. The full-width at half-maximum (FWHM) value is 90 arcsec in comparison with 33 arcsec for the substrate. The occurrence of the Pendellösung fringes indicates interface coherence and high crystallinity of the film. The *c*-axis of the homoepitaxial film is subject to a compressive strain, consistently with the lattice dilation induced by phosphorus. The strains in the epilayer were estimated by asymmetric reciprocal space mapping of the 1 0 $\bar{1}$ 5 reflection of ZnO.

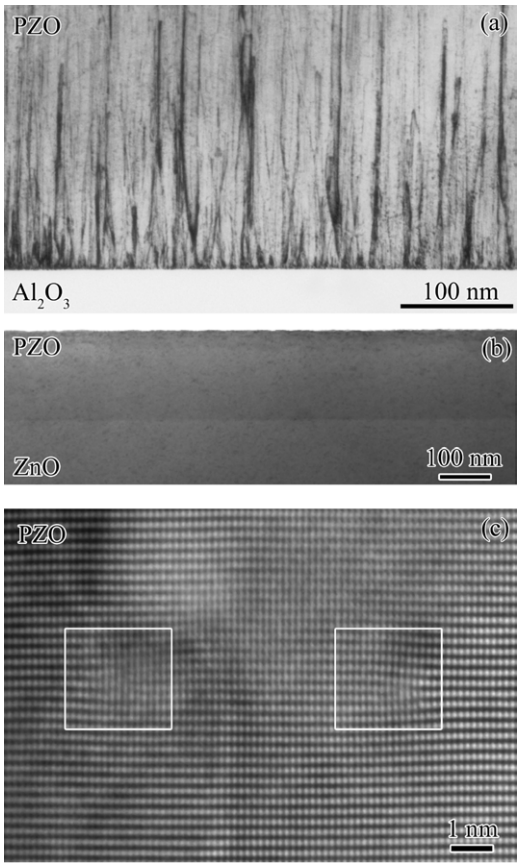

Figure 3. (*a*) Cross-sectional TEM image of p-type heteroepitaxial PZO. The image highlights a high density ($\sim 10^{11}$ cm^{-2}) of threading dislocations. (*b*) Cross-sectional TEM image of p-type homoepitaxial PZO. The image highlights a high density of short interstitial dislocation loop segments. (*c*) Cross-sectional HRTEM image showing the atomic structure of a pair of dislocations belonging to a dislocation loop.

Using the lattice parameters ($c_{ZnO} = 5.2069$ Å and $a_{ZnO} = 3.2495$ Å) of bulk ZnO as reference, the lattice constants of the homoepitaxial PZO film were determined to be $c_{PZO} = 5.2232$ Å and $a_{PZO} = 3.2483$ Å, corresponding to strains $\varepsilon_c = (c_{PZO}/c_{ZnO}) - 1 = 3.1 \times 10^{-3}$ and $\varepsilon_a = (a_{PZO}/a_{ZnO}) - 1 = -3.7 \times 10^{-4}$, corresponding to an increase of only 0.35% in the c/a ratio. Note that the deformation induced by phosphorus is more significant along the growth axis of the epilayer. Figure 2(*b*) is a 0 0 0 2 θ–2θ XRD pattern of a heteroepitaxial p-type PZO film. The film grows epitaxially on sapphire without rotation domains, as confirmed by the asymmetric ϕ-scan of the 1 1 $\bar{2}$ 4 reflection of ZnO shown in figure 2(*c*) and the observed 30% rotation between the ZnO and the sapphire lattices (16.8% lattice mismatch). The FWHM values of the ω-scans of the 0002 and the 1 0 $\bar{1}$ 2 reflections increase from 0.025° and 0.067° for homoepitaxy, respectively, to 0.831° and 1.436° for heteroepitaxy.

The microstructure of heteroepitaxial PZO is shown in figure 3(*a*). The film consists of a high density of threading dislocations ($\sim 1.0 \times 10^{11}$ cm^{-2}) and partial dislocations (7.7×10^{11} cm^{-2}) associated with basal stacking faults. The threading dislocations form because of the large lattice mismatch between ZnO and sapphire and because of the low mobility of the phosphorus atom. The interstitial dislocation loops form by precipitation of zinc interstitials [13] and correspond to type-I intrinsic stacking faults, which have the lowest formation energy among stacking faults in ZnO [14]. The partial dislocations have a Burgers vector $\vec{b} = 1/6\langle 0\,2\,\bar{2}\,3\rangle$ and are therefore of the Frank–Shockley type. Figure 3(*b*) is a cross-sectional TEM image showing the microstructure of homoepitaxial PZO. No threading dislocations are observed. The primary defects appear to be 10–15 nm long segments of interstitial dislocation loops formed by inserting one half of a ZnO unit cell in the basal plane, and their associated partial dislocations. Their density is similar to what we calculated for the heteroepitaxial samples. Figure 3(*c*) is a representative high-resolution TEM micrograph showing the atomic structure of a pair of Frank–Shockley partial dislocations belonging to an interstitial dislocation loop. According to a systematic TEM study of P-doped ZnO thin films, the density of interstitial dislocation loops was found to increase with the concentration of phosphorus, indicating that these defects formed upon P-doping.

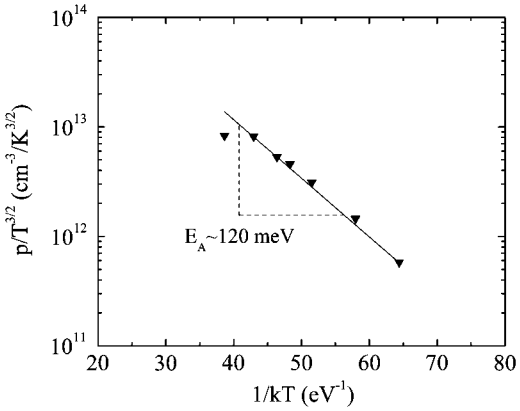

Figure 4. Arrhenius plot of $p/T^{3/2}$ as a function of $1/T$ for p-type heteroepitaxial PZO. The slope gives an acceptor activation energy of ~120 meV.

3.2. Electrical properties

All as-deposited heteroepitaxial films show n-type conductivity, but films grown at 600 °C become p-type after annealing in oxygen atmosphere and have a resistivity of $4.9 \times 10^1\ \Omega$ cm, a Hall mobility of 1 cm^2 V^{-1} s^{-1} and a hole concentration of 1.3×10^{17} cm^{-3} [10]. Figure 4 shows the least squares fit to $p/T^{3/2}$ as a function of $1/T$ for the p-type sample, which gives an acceptor activation energy of 120 ± 30 meV. Since the (0 0 0 1) ZnO substrate used in this work is semi-insulating with a resistivity of $\sim 10^3\ \Omega$ cm, the electrical properties of homoepitaxial PZO films can be measured. All as-grown homoepitaxial PZO films also show n-type conductivity and become p-type after annealing at 600 °C in 1.0 atm O_2. The electrical properties of these samples at room temperature are summarized in table 1.

We fabricated p–n homojunctions on sapphire and ZnO substrates using the process described above to grow the

Table 1. Electrical properties at room temperature of n-type and p-type heteroepitaxial and homoepitaxial PZO films.

PZO sample	Resistivity (Ω cm)	Mobility ($cm^2\ V^{-1}\ s^{-1}$)	Density (cm^{-3})
n-type heteroepitaxial	1.5×10^{-1}	11	3.8×10^{18}
n-type homoepitaxial	1.4×10^{-1}	123	3.5×10^{17}
p-type heteroepitaxial	4.9×10^{1}	1	1.3×10^{17}
p-type homoepitaxial	4.1	8	1.9×10^{17}

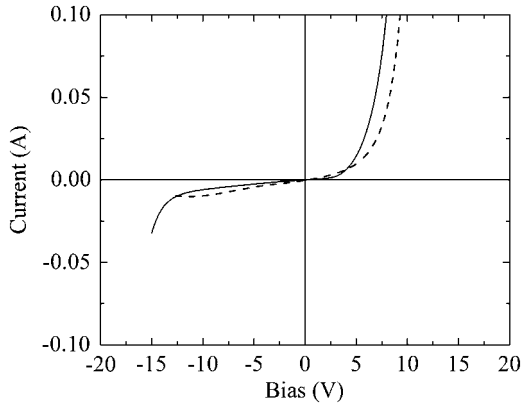

Figure 5. Current–voltage characteristics across p–n homojunctions grown on (*a*) ZnO (——) and (*b*) sapphire (- - - -) substrates.

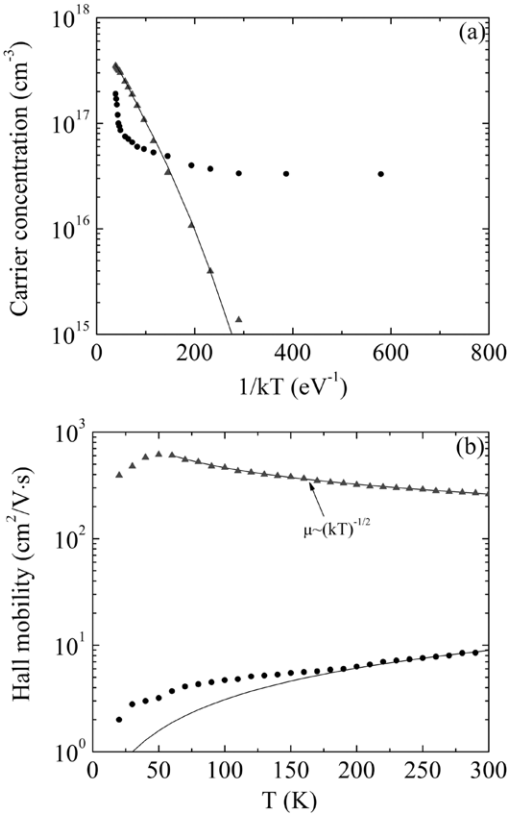

Figure 6. Temperature dependences of (*a*) the carrier concentration and (*b*) the Hall mobility of homoepitaxial PZO films before annealing (▲) and after annealing in O_2 (●). The solid lines are the fits.

p-type layer. The n-type layer was a 1 μm thick phosphorus-doped ZnO layer grown at 800 °C with a resistivity of $3.6 \times 10^{-2}\ \Omega$ cm, a Hall mobility of $52\ cm^2\ V^{-1}\ s^{-1}$, and an electron concentration of $3.4 \times 10^{18}\ cm^{-3}$. Before measuring the current–voltage characteristic across the junction, the contact ohmic linearity was verified. Figure 5 shows the I–V characteristics across the homojunctions grown on sapphire (dashed line) and on ZnO (solid line). The homojunction grown on ZnO exhibits a clearly defined rectifying behaviour. A fit to the Shockley diode equation gives a turn-on voltage of ~6 V and an ideality factor of 1.7 ± 0.2. Note that the junction has a breakdown voltage of 13 V with a leakage current that increases slightly under increasing reverse bias.

Despite the good I–V characteristic obtained for the p–n homojunction grown on the ZnO substrate, no electroluminescence (EL) was observed at room temperature. We have identified several roadblocks that may be responsible for the absence of EL. Firstly, the hole concentration in the p-type layer may not be high enough ($<10^{18}\ cm^{-3}$) to turn on any near-band-edge (NBE) emission. Secondly, the role of crystal defects on the device performance is critical. The observation that the leakage current in junctions grown on sapphire is slightly larger than on ZnO highlights the detrimental effect of crystal defects such as threading dislocations on the recombination efficiency and junction property. Furthermore, the high density of threading dislocations in the p-type layer may provide trap centres to radiative recombination, especially since the dislocation spacing, as small as 3 nm in some areas, is much less than the minority carrier diffusion length in p-type ZnO, which is typically on the order of 0.5–1 μm [15]. For the junctions grown on ZnO substrates, the low-angle tilt boundaries observed by XRD at the surface of the substrate may act as leakage paths. In addition, the mobility of dislocation loops upon application of a bias may also degrade the p–n junction, as observed in ZnSe-based devices [16]. In P-doped ZnO, the acceptor complexes responsible for the p-type conductivity are stabilized in the vicinity of the lines of the partial dislocations (see below) and may be destabilized by their motion.

Results from variable-temperature Hall-effect measurements of the homoepitaxial films before (n-type) and after annealing (p-type) are shown in figure 6. The electron concentration of the n-type samples was fitted using the charge balance equation (CBE) and a two donor-one acceptor model [17]. The following donor activation energies and concentrations were obtained: $E_{D_1} = 29$ meV, $N_{D_1} = 5.4 \times 10^{17}\ cm^{-3}$, $E_{D_2} = 40$ meV and $N_{D_2} = 3 \times 10^{16}\ cm^{-3}$ and the acceptor concentration was $N_A = 2 \times 10^{16}\ cm^{-3}$. In contrast, no good fit to the CBE could be obtained for the p-type homoepitaxial sample possibly because of the uncertainty on the degeneracy of holes [18]. Yet, the plateau in the hole concentration suggests initial freezing of the free carriers followed by the gradual ionization of the neutral acceptor.

While Look and Sizelove pointed out that dislocation scattering occurs primarily in epilayers containing at least $10^8\ cm^{-2}$ edge-type threading dislocations [7], the partial dislocations with a Burgers vector $\vec{b} = \frac{1}{6}\langle 0\,2\,\bar{2}\,3\rangle$ can also scatter carriers when charged. We included dislocation scattering in Matthiessen's rule to fit the hole mobility and

found that a good fit could be obtained only between 180 and 300 K, assuming a dislocation density of $\sim 5 \times 10^{11}$ cm^{-2} and a residual donor level concentration of 10^{16} cm^{-3}. Since this dislocation density is on the same order as the density of partial dislocations we calculated by TEM, we suggest that the lines of the partial dislocations become charged as the acceptor complex gradually ionizes above 180 K. The Hall mobility in n-type homoepitaxial PZO shows a maximum $\mu_H = 590$ cm^2 V^{-1} s^{-1} at 60 K and its temperature dependence is almost entirely dominated by piezoelectric scattering. The strength of dislocation scattering is weak possibly because the acceptor complexes are neutral or gettered at the dislocation lines.

3.3. Mechanism of p-type conduction in phosphorus-doped ZnO

We now discuss how the complex forms in the lines of partial dislocations. Due to the large size mismatch between P and O atoms, the P dopants (existing as P_{Zn} antisites [19] and responsible for the n-type conduction observed in as-grown samples) locate preferentially at high surface energy regions such as the dislocation lines; they bind with two zinc vacancies to form a complex defect P_{Zn}–$2V_{Zn}$ to relieve the strain energy associated with the P_{Zn} antisites, as predicted by theory [8]. Such complex acts as shallow acceptor that ionizes enough holes provided the native donor concentration is reduced by post-deposition annealing. As the phosphorus antisite binds with two zinc vacancies, the equilibrium concentration of zinc vacancies decreases, hence the injection of zinc vacancies and the formation of Frenkel pairs to balance the charge. The precipitation of zinc interstitials is the reason why interstitial dislocation loops form. Therefore, it can be concluded that the existence of phosphorus doping and complex formation induce interstitial dislocation loops and type-I stacking faults, hence the higher density of such defects in P-doped ZnO films than in undoped ZnO films. In addition, the gettering of shallow donors such as zinc interstitials by the defects results in a lower electron concentration and minimizes hole compensation effects.

3.4. Optical properties

Figure 7 shows the PL spectra at 12.5 K of the p-type homoepitaxial and heteroepitaxial PZO layers. For comparison, the PL spectra of bulk ZnO and of undoped ZnO/Al_2O_3 grown at 600 °C are also shown. Their NBE luminescence is dominated by free and bound excitons along with their excited states and phonon replicas. The NBE luminescence of both PZO layers is dramatically quenched and broadened due to the high density of non-radiative recombination centres induced by the phosphorus dopant. Note that there is an obvious strain effect in the phosphorus-doped epilayers based on the deformation potential induced by phosphorus. The NBE luminescence of the homoepitaxial layer features two donor-bound excitons at 368.2 and 368.5 nm, and is dominated by a 372.5 nm transition, which we tentatively assign to a defect-related transition (Y-line) based on exclusion principles. Since the dominant defects in PZO/ZnO layers

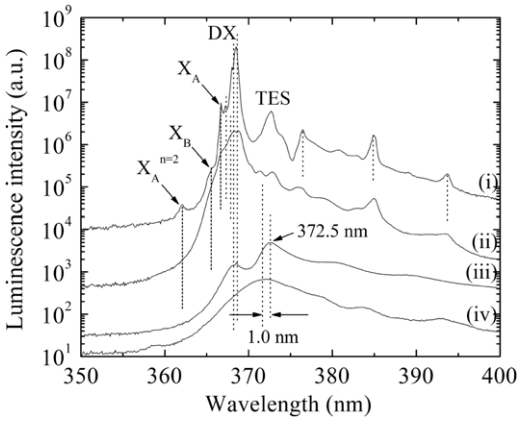

Figure 7. PL spectra at 12.5 K of (i) the ZnO substrate used in this study, (ii) heteroepitaxial ZnO deposited on (0 0 0 1) sapphire, (iii) p-type homoepitaxial PZO and (iv) p-type heteroepitaxial PZO. The comparison shows that the crystal defects induced by phosphorus doping quench the luminescence yield.

are the interstitial dislocation loops, the 372.5 nm Y-line may be related to excitons bound to these defects. In conclusion, while heavy phosphorus doping is necessary to obtain p-type conductivity, it dramatically degrades the epilayer photoluminescence. One solution to minimize non-radiative recombination is to lower the phosphorus concentration in the film while ensuring annihilation of native donors, possibly with the help of an O_2 plasma during growth.

4. Conclusion

The microscopic defects in phosphorus-doped ZnO films epitaxially grown on the (0 0 0 1) sapphire and the (0 0 0 1) ZnO substrates and their effects on the electrical properties were studied. We suggest that edge-type dislocations associated with interstitial dislocation loops provide a mechanism for zinc vacancy injection and relieve the buildup in the strain energy associated with the antisite defect. This results in the formation and stabilization of P_{Zn}–$2V_{Zn}$ shallow acceptors that can lead to p-type conductivity due to the annihilation of native donors by gettering and out-diffusion from the dislocation cores.

Acknowledgments

This work was supported by the National Science Foundation (NSF) through Grant Nos DMR 0308012 and DMR-0315633, by NSFC Contract No. 50428202 and by IMRA America, Inc.

References

[1] Nakamura S, Senoh M and Mukai T 1993 *Japan. J. Appl. Phys.* **32** L8
[2] Ryu Y R, Lubguban J A, Lee T S, White H W, Jeong T S, Youn C J and Kim B J 2007 *Appl. Phys. Lett.* **90** 131115
[3] Makino T, Segawa Y, Kawasaki M, Ohtomo A, Shiroki R, Tamura K, Yasuda T and Koinuma H 2001 *Appl. Phys. Lett.* **78** 1237
[4] Ohtomo A, Kawasaki M, Koida T, Masubuchi K, Koinuma H, Sakurai Y, Yoshida Y, Yasuda T and Segawa Y 1998 *Appl. Phys. Lett.* **72** 2466

[5] Ryu Y R, Lee T S, Lubguban J A, Corman A B, White H W, Leem J H, Han M S, Park Y S, Youn C J and Kim W J 2006 *Appl. Phys. Lett.* **88** 052103
[6] Ponce F A, Bour D P, Götz W and Wright P J 1997 *Appl. Phys. Lett.* **68** 57
[7] Look D C and Sizelove J R 1999 *Phys. Rev. Lett.* **82** 1237
[8] Limpijumnong S, Zhang S B, Wei S H and Park C H 2004 *Phys. Rev. Lett.* **92** 155504
[9] Lee W J, Kang J and Chang K J 2006 *Phys. Rev.* B **73** 024117
[10] Allenic A, Guo W, Chen Y B, Katz M B, Zhao G Y, Che Y, Hu Z D, Liu B, Zhang S B and Pan X Q 2007 *Adv. Mater.* **19** 3333
[11] Williamson G K and Hall W H 1953 *Acta Metall.* **1** 22
[12] Dunn C O and Koch E F 1957 *Acta Metall.* **5** 548
[13] Gerthsen D, Livitnov D, Gruber Th, Kirchner C and Waag A 2002 *Appl. Phys. Lett.* **81** 3972
[14] Yan Y, Dalpian G M, Al-Jassim M M and Wei S H 2004 *Phys. Rev.* B **70** 193206
[15] Lopatiuk-Tirpak O *et al* 2006 *J. Appl. Phys.* **100** 086101
[16] Guha S, Cheng H, Haase M A, Depuydt J M, Qiu J, Wu B J and Hofler G E 1994 *Appl. Phys. Lett.* **65** 801
[17] Look D C 1989 *Electrical Characterization of GaAs Materials and Devices* (New York: Wiley)
[18] Look D C, Renlund G M, Burgener R H II and Sizelove J R 2004 *Appl. Phys. Lett.* **85** 5269
[19] Wahl U, Rita E, Correia J G, Marques A C, Alves E and Soares J C 2006 *Phys. Rev. Lett.* **95** 215503